Study on the photoinitiation mechanism of carbazole-based oxime esters (OXEs) as novel photoinitiators for free radical photopolymerization under near UV/visible-light irradiation exposure and the application of 3D printing

Ji Feng, Yijun Zhang, Di Zhu, Fabrice Morlet-Savary, Michael Schmitt, Bernadette Graff, Pu Xiao, Frédéric Dumur, Jacques Lalevée

Study on the photoinitiation mechanism of carbazole-based oxime esters (OXEs) as novel photoinitiators for free radical photopolymerization under near UV/visible-light irradiation exposure and the application of 3D printing

Ji Feng [a,b], Yijun Zhang [a,b], Di Zhu [c], Fabrice Morlet-Savary [a,b], Michael Schmitt [a,b], Bernadette Graff [a,b], Pu Xiao [c]*, Frédéric Dumur [d]* and Jacques Lalevée [a,b]*

[a] Université de Haute-Alsace, CNRS, IS2M UMR7361, F-68100 Mulhouse, France.

[b] Université de Strasbourg, France.

[c] Research School of Chemistry, Australian National University, Canberra, ACT 2601, Australia.

[d] Aix Marseille Univ, CNRS, ICR, UMR 7273, F-13397 Marseille, France.

Abstract:

In this work, twenty-two oxime esters bearing different functional groups and based on carbazole as the chromophore were designed and synthesized as Type I photoinitiators. Interestingly, all structures mentioned in this work have never been reported before (even for their synthesis). These oxime esters were found to have good light absorption properties in the UV-visible range, and especially at 405 nm which is a reference wavelength in photopolymerization. Noticeably, several structures showed better photoinitiation abilities than the benchmark photoinitiator i.e. diphenyl(2,4,6-trimethylbenzoyl)phosphine oxide (TPO), evidencing the interest of these structures. In order to investigate the photoinitiation mechanism of the two series of oxime esters differing by the position of the photocleavable groups, electronic absorption spectra were determined by molecular modeling and density functional theory calculations. Photopolymerization abilities of the different oxime esters and release of CO_2 during the polymerization experiments were determined by Real-Time Fourier Transformed Infrared (RT-FTIR). Active free radicals were characterized by mean of Electron Spin Resonance Spin Trapping (ESR-ST) experiments. On the basis of these different

complementary experiments, chemical mechanisms occurring during photopolymerization could be proposed. Experimental results showed that the decarboxylation reaction occurring subsequent to the photocleavage of oxime esters had a beneficial effect on the photoinitiation ability. Finally, 3D printed objects were successfully obtained by using oxime esters exhibiting the best photoinitiating abilities.
Keywords: Type I photoinitiators; Oxime esters; Photochemical mechanisms; 3D printing; carbazole.

1. Introduction:

The development of green and sustainable chemistry processes constitutes the main research directions of future chemistry. Contrarily to the traditional thermal polymerization that is mostly performed in organic solvents [1], photopolymerization can be carried out in solvent-free conditions so that emission of volatile organic compounds (VOCs) can be considerably reduced.[2] From this viewpoint, photopolymerization constitutes a greener and more environmentally friendly polymerization technique than the traditional thermal polymerization [3]. Thanks to the abovementioned advantages, photopolymerization has been used in applications such as coatings [4], biomedical materials [5], food packaging [6], 3D printing [7-10] and many other research fields, supported by the numerous advantages of photopolymerization such as high efficiency [11], energy saving and environmentally friendly conditions [12]. Nowadays, visible light polymerization is more extensively studied than UV photopolymerization [13], visible light photopolymerization offering the possibility to use light sources that are safer for the manipulator than UV light sources [14]. As drawback, visible photons are less energetic than UV photons so that visible light polymerization is currently lacking efficient photoinitiators.

In photopolymerization, photoinitiator (PIs) is the key element as it can produce radicals or ions by interacting with light [2, 15, 16]. Compared to Type II PIs which can only produce initiating species by mean of a multi-step initiation process involving a bimolecular interaction of the photoinitiator with a co-initiator [16], Type I PIs can

generate active free radicals without any additives, by homolytic cleavage of a selected chemical bond [17]. Considering that the homolytic cleavage is the result of an intramolecular reaction and not from a diffusion-controlled bimolecular interaction which is typically observed with Type II photoinitiators, efficiency of the initiation step is thus less dependent of parameters such as the concentration of the additives/oxygen or the viscosity of the monomers [1]. Among all Type I photoinitiators reported in the literature, oxime esters (OXEs) can initiate a polymerization by homolytic cleavage of the N-O bond. Subsequent to the formation of iminyl and acyloxy/aryloxy radicals, a decarboxylation reaction of the acyloxy/aryloxy radicals can occur [18], producing active free radicals [19] The decarboxylation step is an important step for oxime esters [18, 20, 21]. Indeed, by converting acyloxy/aryloxy radicals as alkyl/aryl radicals, no radical recombination with iminyl radicals can occur, additionally the generated carbon centered radicals are more reactive towards monomers. Parallel to this, release of CO_2 within the resin contribute to impede oxygen diffusion, enabling to address the oxygen inhibition issue and to improve the monomer conversion. Over the years, various chromophores have been investigated, as exemplified with triphenylamines [22], pyrenes, anthracenes [23], naphthalenes [24], chalcones [25], coumarins [19], phenothiazines [26], fluorophenyls [27] and other chromophores. In 2020, Ding and his group [27] designed and synthesized OXEs based on the fluorophenyl scaffold and successfully initiated the photopolymerization of tripropylene glycol diacrylate under the irradiation of LED@395 nm with good conversion rates. However, absorptions of these OXEs remained strongly UV-centered. Concerning benchmark OXEs, numerous structures can furnish high monomer conversions. As drawback, their absorptions are centered in the UV range, as exemplified with *O*-benzoyl-α-oxooxime and *O*-acetyloxime for which absorption maxima located at 314 and 335 nm can be respectively determined [28]. If high monomer conversions could be obtained with these structures, high-intensity ultraviolet light sources had to be used,[29] constituting a severe limitation especially in the present context of energy sobriety that is imposed by numerous countries. Alternatives to these high-intensity ultraviolet light sources are thus

researched [17, 30], and in this field, light emitting diodes (LEDs) have the advantages of being light sources of low cost, exhibiting long operating lifetimes, compactness, robustness and easy availability [1, 31]. At present, these relatively cheap devices are more and more used by researchers and now replace the traditional mercury lamps that will be not allowed to be fabricated, imported and exported by the treaty established during the Minamata Convention on Mercury in 2013 [32, 33]. However, considering that the absorption spectra (*O*-benzoyl-α-oxooxime OXE 01, λ_{max} = 326 nm, *O*-acetyloxime OXE 02, λ_{max} = 338 nm) [18] of commercial OXEs do not match the emission spectrum of near-UV-visible LEDs (between 365 and 425 nm) [28, 33], a great deal of effort remains to be done in order to design the next generation OXEs that can be activated in the near UV/visible range. Therefore, it is very meaningful to design and synthesize new OXEs, and to investigate their photoinitiating abilities at long absorption wavelengths [34]. If the absorption properties of photoinitiators is a key parameter governing their reactivities, their solubilities in resins is also important in order the photoinitiator to efficient interact with additives (in the case of Type II photoinitiators), or directly with the monomer (in the case of Type I photoinitiators). With aim at improving the solubility in resins, two distinct strategies can be used. The first one consists in introducing solubilizing chains (generally long alkyl chains) and the second one to introduce functional groups capable to drastically reduce π-π interactions and therefore aggregation. In this field, *tert*-butyl groups, by their tridimensional structures, can easily address the aggregation issue and this strategy is commonly used in Organic Electronics for the design of solution-processed devices or for the design of fluorescent probes. This strategy can also be used in photopolymerization and the two families proposed in this work aim at designing photoinitiators that can be facilely dissolved in resins. This strategy is pertinent, especially, if polyaromatic structures are designed, as done in this work. Noticeably, for the design of the two series of dyes, *N*-ethylcarbazole with its short ethyl chain was selected as the appropriate starting material used for the design of two series of photoinitiators bearing one or two *tert*-butyl groups.

In this work, a series of twenty-two OXEs bearing different substituents were

successfully synthesized and characterized. Chemical structures of the different OXEs are presented in Figures 1 and 2. Based on carbazole as the chromophore, these OXEs were categorized into two series (B series and C series), differing by the number of *tert*-butyl groups and the position of the photocleavable group. By combining molecular orbital calculation, time dependent density functional theory, free radical photopolymerization (FRP), UV-visible absorption and fluorescence spectroscopy, steady-state photolysis, fluorescence excited state lifetime and electron spin resonance spin trapping (ESR-ST) experiments, photoinitiation abilities of the different OXEs and the mechanisms of polymerization could be established. Finally, as an application, 3D printing experiments were carried out using the best investigated photoinitiator.

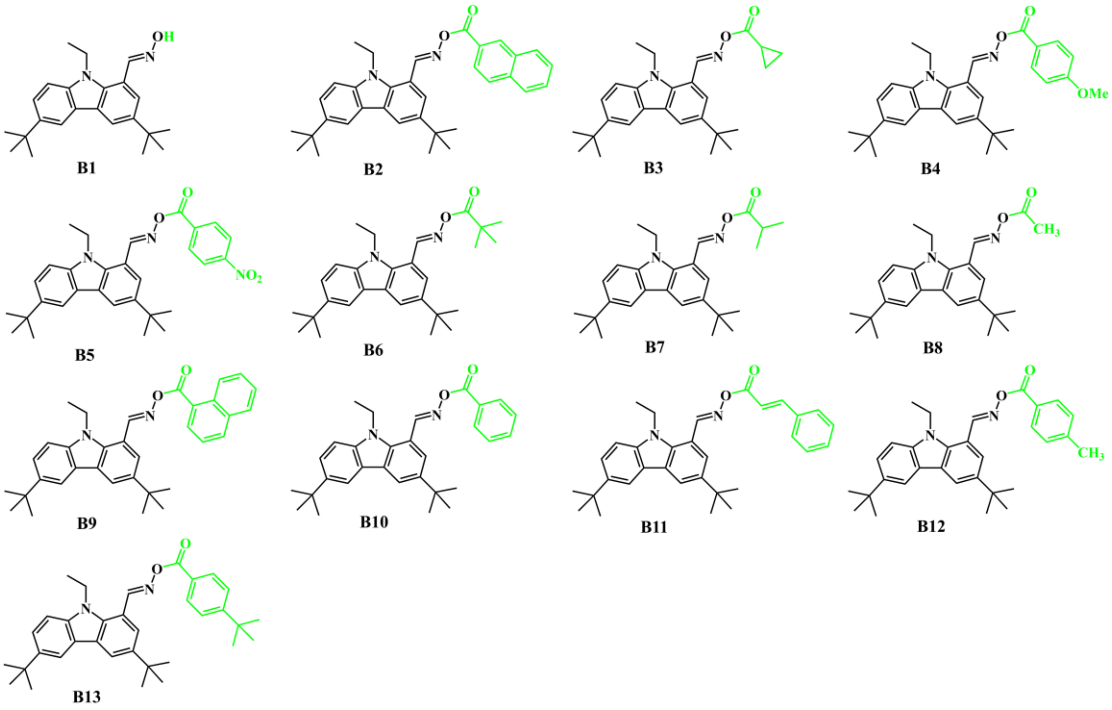

Figure 1. Chemical structures of OXEs B1-B13 (B series).

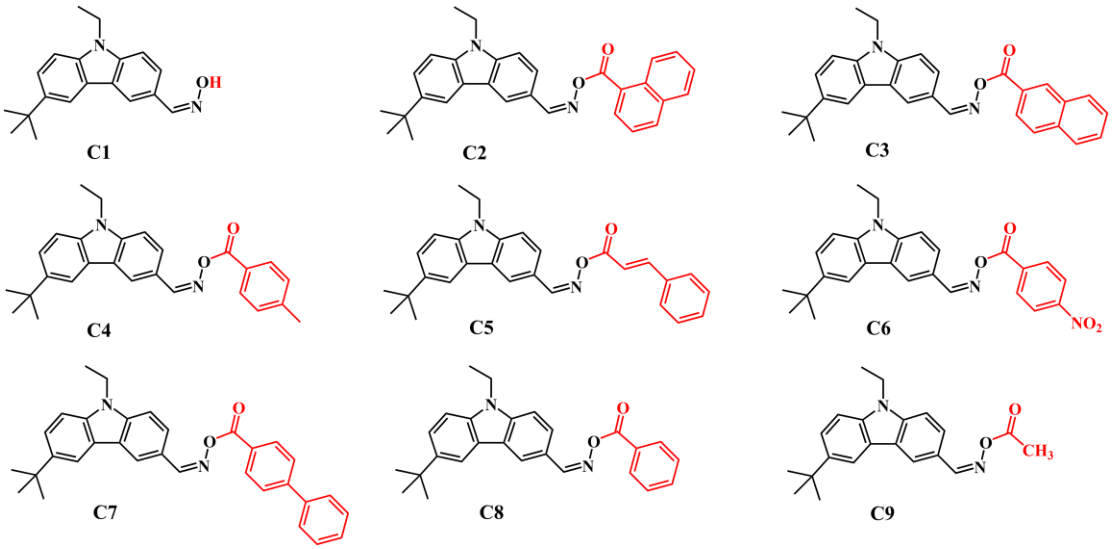

Figure 2. Chemical structures of OXEs C1-C9 (C series).

2. Experimental Section

2.1 Materials

The different OXEs used for photopolymerization have been synthesized by our group (see below part 3.1 and in supporting information). The benchmark monomer i.e. trimethylolpropane triacrylate (TMPTA) used for photopolymerization was purchased from Sartomer (France). The benchmark photoinitiator diphenyl(2,4,6-trimethylbenzoyl)-phosphine oxide (TPO) used for comparison was purchased from Lambson Ltd. (United Kingdom). The colloidal silica suspension (LUDOX-AS-30, 30 wt% suspension in H_2O) was obtained from Sigma-Aldrich. The free radical trapping agent phenyl-*N*-*tert*-butyl nitrone (PBN) used for ESR experiments was obtained from TCI-Europe (France).

2.2 Sample preparation

OXEs and TMPTA were successfully added into a small glass bottle with a stopper and the resulting resin was stirred with a magnetic rotor until the PIs was completely dissolved in the monomer. It was stored in a dark environment before photopolymerization. Here, the weight percentage of OXEs was kept at 0.5 %phr relative to TMPTA. All thin samples were dropped in laminate between two polypropylene films with one drop of resin deposited (See Figure S1(a)). All thick samples were dropped into a circular top with grooves with five drops deposited (See

Figure S1(b)).

2.3 Light Absorption Spectrum and Steady-state Photolysis

UV−visible absorption spectra of the different OXEs were measured with a JASCO V730 spectrometer in 5 × 10^{-5} M solutions in acetonitrile. Steady-state photolysis experiments were carried out by using the same spectrometer. Measurements were performed in acetonitrile under the irradiation of a LED@405 nm (light intensity: 110 mW/cm^2). The concentrations of the different OXEs were 5 × 10^{-5} M.

2.4 Fluorescence Spectrum and Fluorescence Lifetime

Fluorescence spectra of the different OXEs (5 × 10^{-5} M in acetonitrile) were obtained with a spectrofluorometer JASCO FP-750. When the wavelength of excitation was 367 nm and the impulse width was less than 1.4 ns, the lifetime of fluorescence excited-state of PIs was measured by a detector (Instrument model HORIBA PPD-850). The impulse response function (IRF) of the instrument was calculated through the colloidal silicon dioxide suspension LUDOX.

2.5 Photopolymerization Profiles Obtained by RT-FTIR

Photopolymerization kinetics associated to OXEs were studied by RT-FTIR spectroscopy (JASCO FTIR-4700). The resins were added to a plastic mold (Figure S1) and between two polypropylene films for thick (1.4 mm) and thin (25 microns) samples, respectively. The characteristic peak of the acrylate functional group was continuously detected at about 6150 cm^{-1} (thick samples) and 1650 cm^{-1} (thin samples) by RT-FTIR. The photopolymerization profiles were obtained by the equation:

$$Conversion\ (\%) = \frac{A_0 - A_t}{A_0} \times 100\%$$

Where A_0 is the peak area of the acrylate functional group at 0 s and A_t is the peak area of the acrylate functional group at t s.

2.6 ESR-ST experiments

In order to study the free radicals produced during the photopolymerization process, the ESR-ST was carried out by an X- band spectrometer (Bruker EMXplus). Free radicals were trapped by PBN and observed in a nitrogen atmosphere in *tert*-butylbenzene. The concentration of OXEs was 1 × 10^{-4} M. All operations were

performed at room temperature. In addition, the ESR-ST spectra were simulated by the PEST WINSIM program.

2.7 Computational Procedure

For the molecular modelling data, the N−O bond dissociation energy (BDE) and the triplet state energy (E_T) of OXEs were calculated with the density functional theory (DFT) at the UB3LYP/6-31G* level.

2.8 3D printing experiments

The formulations for 3D printing experiments were 0.5% PIs in TMPTA. Then, direct laser write (DLW) experiments were performed with a laser diode at 405 nm (110 mW), and the glass tank used for printing was homemade (about 2 mm thickness). The printed pattern was observed by a digital camera.

3. Results and Discussion

3.1 Synthesis of the OXEs

Syntheses of all OXEs are described in Scheme 1. First, 9-ethyl-9*H*-carbazole (a1) and 3,6-di-*tert*-butyl-9-ethyl-9*H*-carbazole-1-carbaldehyde (a3) used as the starting materials for the synthesis of oxime esters were prepared in two steps. By mean of a Friedel-Craft reaction using 2-methylpropane and aluminum chloride, 3,6-di-*tert*-butyl-9-ethyl-9*H*-carbazole (a2) could be prepared in 81% yield. Then, a2 was converted as 3,6-di-*tert*-butyl-9-ethyl-9*H*-carbazole-1-carbaldehyde (a3) by mean of a Vilsmeier-Haack reaction in 48% yield. Interestingly, in the reaction conditions used, no side-products formed and the di(formyl) derivative 3,6-di-*tert*-butyl-9-ethyl-9*H*-carbazole-1,8-dicarbaldehyde (a3') was not detected as structure in the crude reaction mixture. Concerning 6-(*tert*-butyl)-9-ethyl-9*H*-carbazole-3-carbaldehyde (d3), it could be prepared in two steps, first by preparing the aldehyde (d2) that was subjected to a Friedel-Craft reaction with 2-methylpropane, providing the targeted aldehyde (d3) in 68% yield (See Scheme 1). Here again, d2 could be obtained without formation of 9-ethyl-9*H*-carbazole-3,6-dicarbaldehyde (d2'), the synthesis of this dialdehyde being only possible in other reaction conditions.

Oximes B6 and B7 were prepared in one step using aldehydes a3 and d3, sodium acetate and hydroxylamine hydrochloride by using mixed solvents (H_2O, MeOH and THF). The two compounds B1 and C1 could be obtained in quantitative yields. Specifically, the different oximes B1 and C1 were esterified using the appropriate acid chloride derivatives E1-E13 and triethylamine as the base (See Scheme 1). All esters B2-B13 and C2-C9 could be obtained with reaction yields ranging between 66% for B11 up to 92% for C8 (See Table 1). Detailed synthetic procedures of all OXEs are given in the Supporting Information. It has to be noticed that all oxime esters reported in this work have never been previously reported in the literature, evidencing the interest of these structures. Among the starting aldehydes, even the synthesis of 6-(*tert*-butyl)-9-ethyl-9*H*-carbazole-3-carbaldehyde (d3) was not reported in the literature. Only 3,6-di-*tert*-butyl-9-ethyl-9*H*-carbazole-1-carbaldehyde (a3) was mentioned in a paper devoted to the design of position isomers of bicarbazoles.[35]

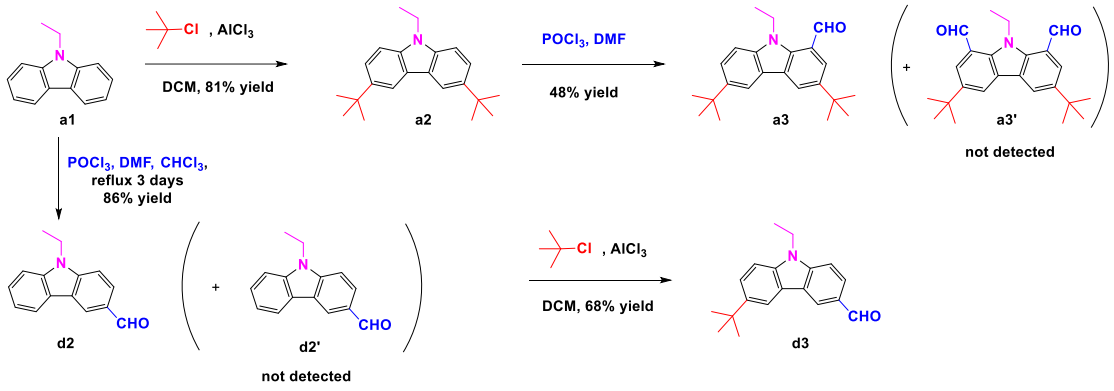

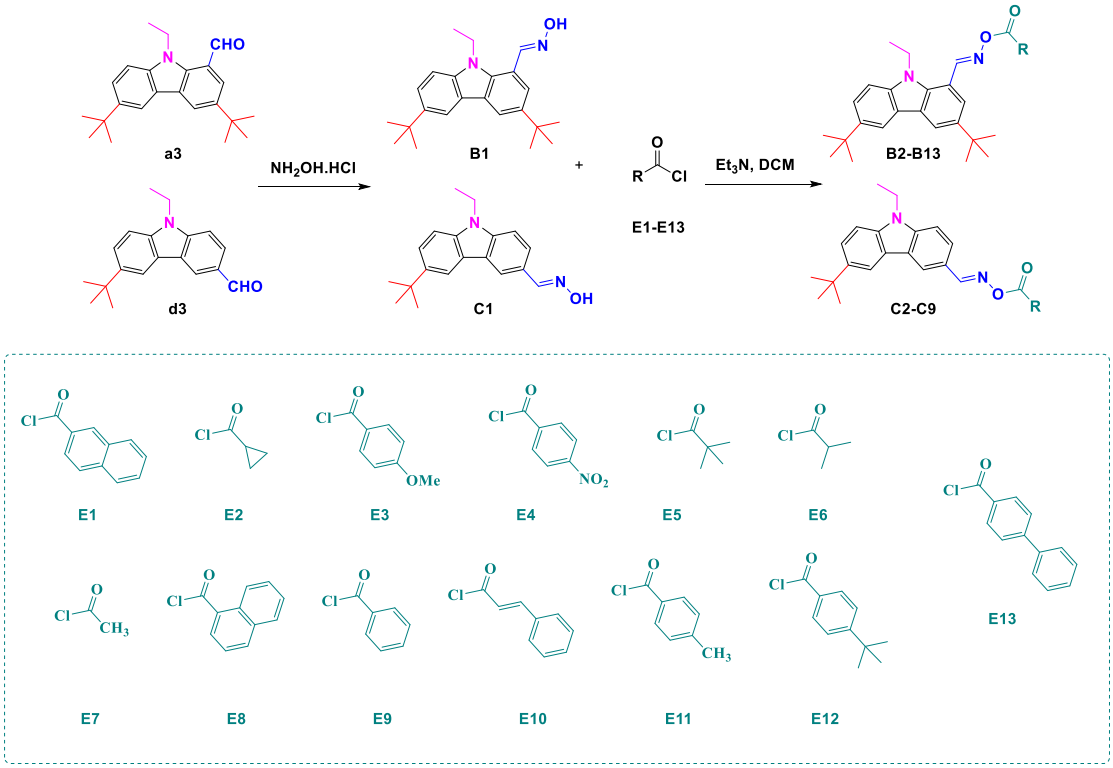

Scheme 1. Synthetic route to the different OXEs B1-B13 and C1-C9.

Table 1. Reaction yields obtained during the synthesis of the different OXEs.

PIs	Reaction yields (%)	PIs	Reaction yields (%)
B1	quant.	C1	quant.
B2	82	C2	82
B3	71	C3	82
B4	87	C4	74
B5	75	C5	71
B6	77	C6	69
B7	86	C7	88
B8	84	C8	92
B9	74	C9	78
B10	68		
B11	66		
B12	88		
B13	88		

3.2 Light Absorption Properties

Due to the presence of the tert-butyl group in the two series of Type I photoinitiators, all dyes exhibited a good solution in acetonitrile. UV-visible absorption

spectra of the different OXEs were thus studied in acetonitrile as the solvent (See Figure 3). Optical characteristics of OXEs are listed in Table 2. Interestingly, all OXEs have good solubilities in acetonitrile at room temperature and this remarkable solubility can be confidently assigned to the presence of tert-butyl groups adversely impacting π-π stacking interactions (See Figure S2). All OXEs displayed a broad absorption band extending up to 400-450 nm. The maximum absorption wavelengths (λ_{max}) of B7 and B8 in series B were 374 and 372 nm respectively. The molar extinction coefficients (ε_{max}) at the λ_{max} were 6260 and 6400 $M^{-1}cm^{-1}$, and the molar extinction coefficients (ε_{405nm}) at λ_{405} were 1830 and 1780 $M^{-1}cm^{-1}$, respectively. Compared to compounds B1 and C1 without OXE functional groups, the λ_{max} of OXEs of series B exhibited a red-shifted absorption, while the λ_{max} of OXEs of series C exhibited a blue-shift. To support the redshift detected with oxime esters of series B compared to the parent oxime B1, an electron-withdrawing effect generated by the oxime ester groups was suggested [36]. In the case of the series C, the substituent is introduced in a none-conjugated position with regards to the carbazole scaffold, supporting the hypsochromic shift detected for this series. The above results showed that all OXEs are sensitive to blue light and therefore are appropriate candidates for photopolymerization experiments done at 405 nm but more generally for near UV light.

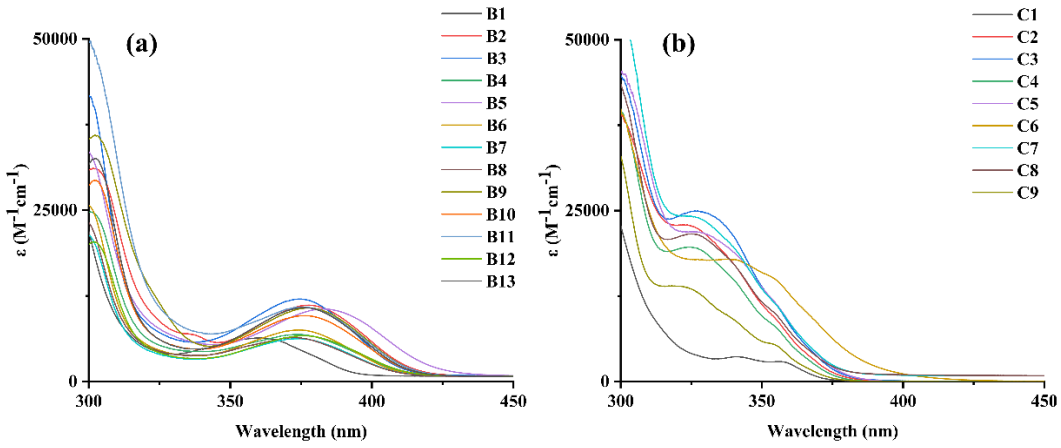

Figure 3. UV-visible absorption spectra of OXEs. (a) OXEs of series B, (b) OXEs of series C in acetonitrile.

Table 2 Light absorption characteristics of OXEs in acetonitrile

PIs	εmax	ε405nm	PIs	εmax	ε405nm

	λ_{max} (nm)	($M^{-1}.cm^{-1}$)			λ_{max} (nm)	($M^{-1}.cm^{-1}$)	
B1	360	6360	8502	C1	340	3590	60
B2	377	11130	4130	C2	323	22860	15
B3	374	12040	3140	C3	327	24950	60
B4	374	6860	2250	C4	325	19680	0
B5	382	10570	6240	C5	327	21880	0
B6	374	7520	2060	C6	338	17900	790
B7	374	6260	1830	C7	324	24160	890
B8	372	6400	1780	C8	325	21610	950
B9	377	10730	3880	C9	319	13980	0
B10	376	9600	3280				
B11	375	10880	3770				
B12	376	6660	2350				
B13	376	10780	3480				

3.3 Free Radical Photopolymerization

Photoinitiation abilities of the different OXEs and the commercial/benchmark PI TPO were examined using TMPTA as a trifunctional monomer. RT-FTIR was used as the appropriate technique to monitor the monomer conversions and thus to establish the photopolymerization profiles of thin and thick samples when exposed to a 405 nm LED.

Photopolymerization profiles of thick samples are presented in Figure 4, and the final functional acrylate conversions (FCs) of OXEs/TMPTA are listed in Table 3. As shown in Figure 4, photoinitiation abilities of OXEs of the B series were better than that of those C series. Among them, B3, B6, B7 and B8 exhibited the highest FCs (68-69%). The polymerization rates (Rp) are very similar to those of TPO (Figure 4). This is directly related to the fact that these OXEs comprise alkyl substituents on the oxime ester moiety, and especially methyl substituents. Indeed, after photocleavage, acetyl groups are prone to decarboxylation, generating methyl radicals that are well-reported to be highly reactive radicals[37]. Photopolymerization profiles of thin samples are shown in Figure S3. As can be seen in this figure, the B series showed high conversion rates, some of which were similar to that of TPO (See Figure S3(a)). In the C series, the

photopolymerization could be initiated only for four samples, and the FCs of OXEs/TMPTA were below 55% (See Figure S3(b)).

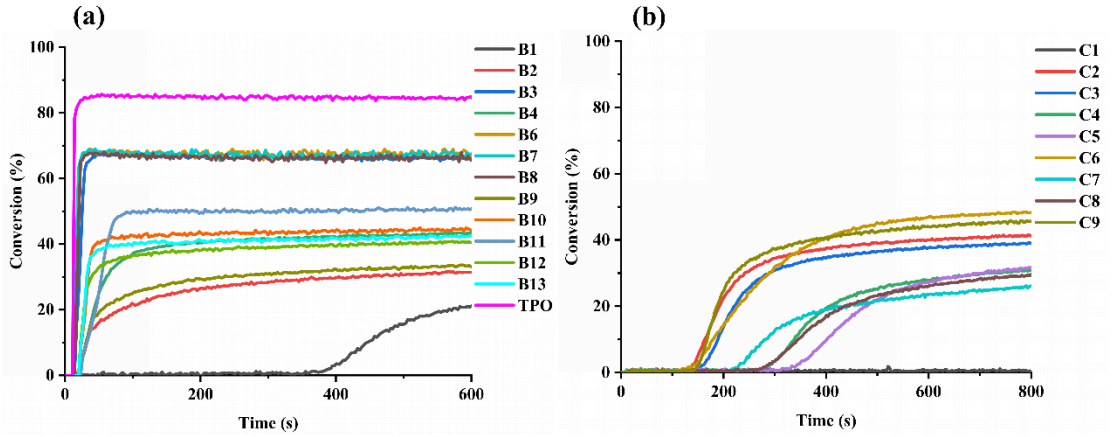

Figure 4. Photopolymerization profiles of TMPTA in the presence of 0.5 phr OXEs for thick sample (about 1.4 mm) upon exposure to LED@405 nm irradiation. The irradiation starts at t = 10 s: (a) OXEs of series B; (b) OXEs of series C.

Table 3. FCs of TMPTA in the presence of OXEs

PIs	FCs (%)	PIs	FCs (%)
B1	21	C2	42
B2	32	C3	39
B3	68	C4	31
B4	44	C5	32
B6	69	C6	48
B7	69	C7	26
B8	68	C8	30
B9	34	C9	46
B10	45	TPO	84
B11	51		
B12	41		
B13	43		

3.4 Steady-State Photolysis

In order to investigate the chemical mechanism of OXEs in photopolymerization, OXEs were dissolved in acetonitrile and the resulting solutions were exposed to a LED@405 nm for steady-state photolysis measurements (See Figure 5). Steady-state photolysis profiles of OXEs are shown in Figures S4 and S5. For B7 and B8, as shown

in Figure 5, by increasing the irradiation time of LED@405 nm, the absorption intensity of B7 at λ_{max} = 374 nm and that of B8 at λ_{max} = 372 nm decreased obviously, and these two compounds were rapidly photolyzed during the first 10 s and photolysis weakens after 60 s of irradiation. Modification of the absorption spectra can be confidently assigned to the homolytic cleavage of the N-O bond in OXEs upon irradiation [5]. Conversely, in the case of oximes B1 and C1, (See Figure S4 and S5), after long-time irradiation, absorption intensities at λ_{max} did not decrease obviously, indicating that no photocleavage occurred with these structures [36].

In order to obtain the singlet excited state energy (E_{S1}) of B7, fluorescence emission spectra and UV-visible absorption spectra were recorded in acetonitrile, so that the singlet excited state (E_{S1}) could be obtained from the intersection point between the absorption and the emission spectra (See Figure 6). E_{S1} of the other OXEs are given in Figures S6 and S7. As shown in Table 4, enthalpies of the N-O bond-breaking process of all OXEs ($\Delta H_{cleavage\ S1}$ = BDE (N-O) - E_{S1} and $\Delta H_{cleavage\ T1}$ = BDE (N-O) - E_{T1}) [36] from E_{S1} or E_{T1} were calculated. In addition, except for B1 and C1, $\Delta H_{cleavage\ S1}$ for all OXEs were negative, indicating that the cleavage of oxime esters can energetically occur from the singlet excited state. Fluorescence lifetimes of OXEs were also measured (See Figure 6 and Figures S8 and S9). Generally, OXEs with short excited state lifetimes exhibited high initiation efficiencies, which is beneficial to the bond breaking process. However, negative $\Delta H_{cleavage\ T1}$ values were also calculated so that photocleavage from the triplet excited state can't be ruled out.

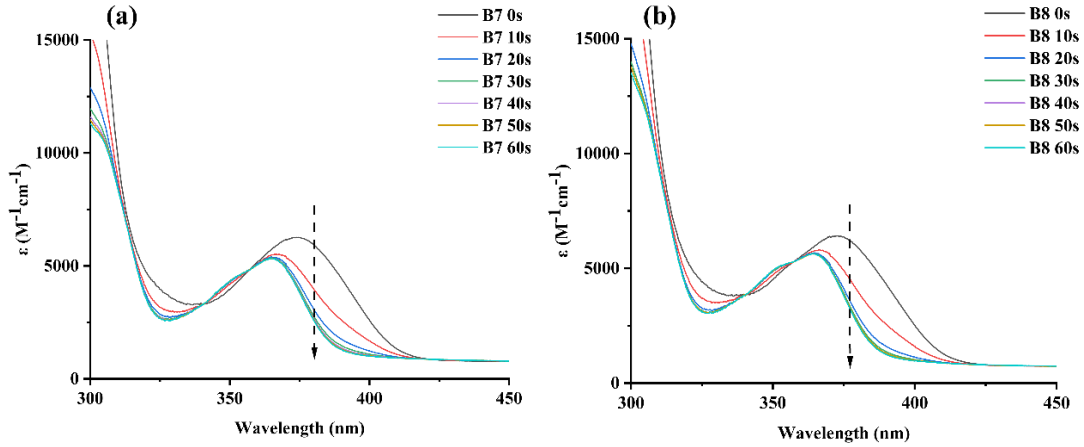

Figure 5. Steady-state photolysis of OXEs under LED@405 nm. (a) B7, (b) B8.

Table 4. Reference parameters of the OXEs B and C series

PIs	N-O BDE	E_{S1}	$\Delta H_{cleavage\ S1}$	E_T	$\Delta H_{Cleavage\ T1}$
	(kcal mol^{-1})				
B1	64.74	74.27	-9.53	52.15	12.59
B2	45.49	73.70	-28.21	59.75	-14.26
B3	47.68	72.94	-25.26	53.40	-5.72
B4	44.99	72.57	-27.58	48.72	-3.73
B5	47.62	72.03	-24.41	49.60	-1.98
B6	44.30	72.21	-27.91	48.45	-4.15
B7	47.92	72.03	-24.29	53.86	-5.94
B8	48.44	72.94	-24.50	53.19	-4.75
B9	42.31	72.94	-30.63	57.96	-15.65
B10	42.83	73.70	-30.87	52.42	-9.59
B11	47.75	72.76	-25.01	52.59	-4.84
B12	42.57	73.89	-31.32	52.37	-9.80
B13	42.67	73.89	-31.22	53.10	-10.43
C1	64.55	78.99	-14.44	50.52	14.03
C2	46.54	80.10	-33.56	57.16	-10.62
C3	47.82	78.34	-30.52	59.83	-12.01
C4	47.92	78.99	-31.07	53.15	-5.23
C5	48.90	79.21	-30.31	53.03	-4.13
C6	50.44	78.56	-28.12	58.27	-7.83
C7	48.11	79.43	-31.32	65.26	-17.15
C8	48.22	79.43	-31.21	53.26	-5.04
C9	48.72	80.10	-31.38	53.55	-4.83

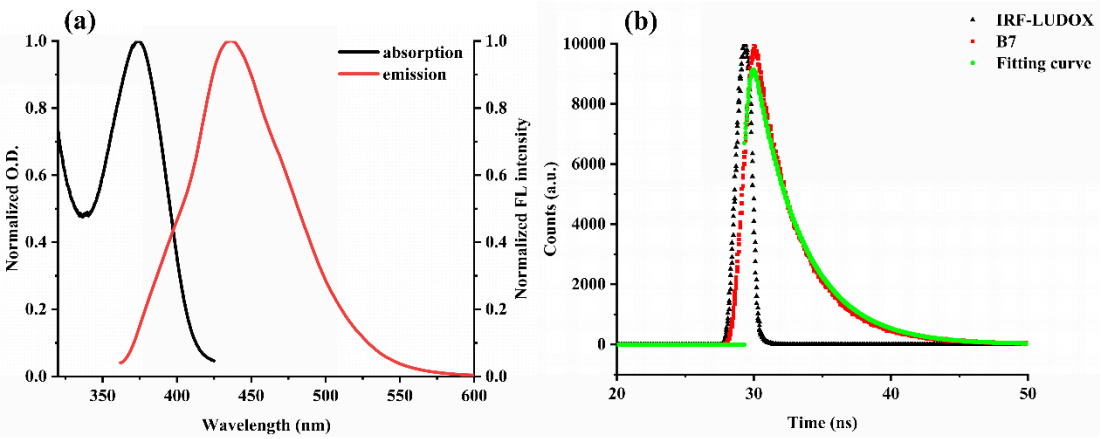

Figure 6. (a) Fluorescence emission spectrum and UV- visible absorption spectrum of B7, (b) fluorescence decay curve of B7.

3.5 Decarboxylation Reaction

Occurrence of a decarboxylation reaction (or not) was evidenced by monitoring the production of CO_2 subsequent to the homolytic cleavage of the N-O bond by RT-FTIR. From the Figures 7(a) and (b), in the B7 and B8 systems respectively, a new characteristic peak can be detected at 2337 cm^{-1} after 60 s of irradiation. For most of the OXE/TMPTA systems, appearance of a new characteristic absorption peak at 2337 cm^{-1} corresponding to CO_2 could be evidenced, but not for all OXEs/TMPTA systems, as shown in Figures S10 and S11. These experimental phenomena can provide evidence of a decarboxylation process. A direct link between polymerization efficiency and CO_2 release can be given i.e. efficient OXEs are associated with cleavage processes and decarboxylation reactions.

On the other hand, the enthalpy for decarboxylation reactions ($\Delta H_{decarboxylation}$) can also provide evidence for decarboxylation[37]. In our previous works, the enthalpy of decarboxylation reaction of a series of acyloxyl radicals was reported by our group. According to the previous research of our group[37], when $\Delta H_{decarboxylation} < 0$ kcal.mol^{-1}, the decarboxylation process is easy to occur (and CO_2 is experimentally observed in RT-FTIR experiments). It thus supports the fact that the decarboxylation of the B8 /TMPTA system is favorable. When $\Delta H_{decarboxylation} > 0$ kcal.mol^{-1}, the decarboxylation process is unfavorable, so that the formation of CO_2 could not be detected in the RT-FTIR spectra of the B2/TMPTA, B11/TMPTA and B12/TMPTA systems. Occurrence (or not) of a decarboxylation reaction of the acyloxy/aryloxy radicals subsequent to their formations can thus be fully explained and anticipated by theoretical calculations.At the same time, this increase in absorbance can be observed for all systems that generate CO_2 (See Figures S10 and S11).

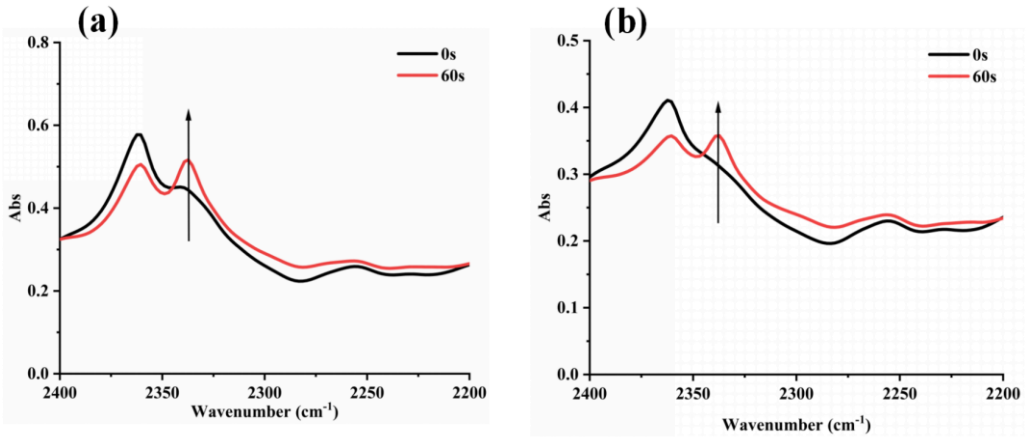

Figure 7. Infrared spectra of (a) B7/TMPTA and (b) B8/TMPTA at t = 0 and 60 s.

3.6 ESR-ST Experiments

By homolytic cleavage of oxime esters, active free radicals can be produced, which constitute the initiating species. To investigate the chemical structures of these radicals, ESR-ST experiments were carried out on two different systems, namely B7 and B8 (See Figure 8). After irradiation at 405 nm for 5 s, two kinds of free radicals could be captured by the free radical scavenger PBN in B7 and B8 systems. For the B7 system (See Figures 8a and 8b), the hyperfine coupling constants for one free radical (97.4%) were α_N = 13.7 G and α_H = 1.7 G. It may be assigned to the acetyloxy radical ($CH_3COO\bullet$) [36]. Hyperfine coupling constants for another one free radical (2.6%) were determined as being α_N = 13.7 G and α_H = 4.8 G, it may be ethyl radical [36]. In the B8 system (See Figures 8c and 8d), only one free radical was detected (See Figure 8b) after 5 s of irradiation. Its hyperfine coupling constants were α_N = 13.5 G and α_H = 1.8 G and it may be assigned to the acetyloxy radical ($CH_3COO\bullet$) [36]. In addition, the experimental results obtained by ESR-ST evidenced the formation of acetoxy radicals. Cleavage of the N-O bond in these different systems is also proved.

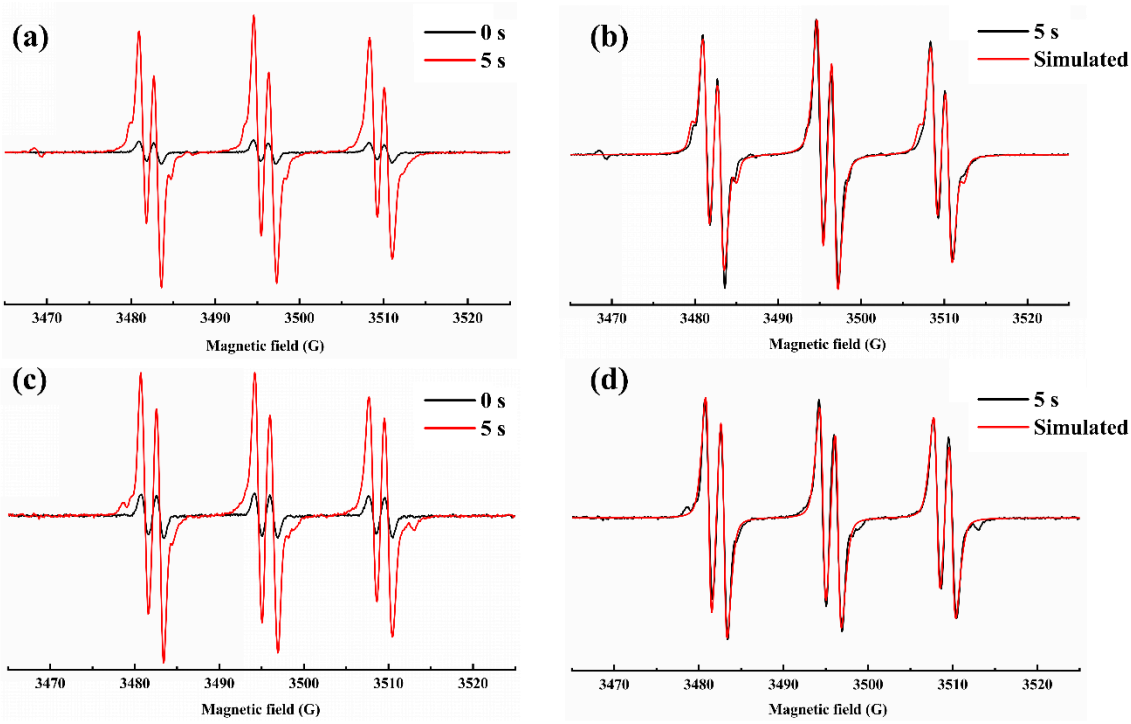

Figure 8. ESR-ST spectrum of the radical adducts (in tert-butylbenzene). (a) and (b) B7, (c) and (d) B8 under LED@405 nm irradiation.

3.7 Photoinitiation Step Mechanisms of OXEs

Through the above experimental results, the chemical mechanisms of photoinitiated polymerization can be proposed and the mechanism is summarized in Scheme 2. When OXEs were exposed to light, the chromophore was excited from the ground state to the excited state. The N-O bond of OXEs could cleave homolytically, producing acyloxy and iminyl radicals (reaction ①). Then, acyloxy radicals can decarboxylate, producing active radicals that can induce monomer polymerization. Parallel to this, CO_2 is released (reaction ②).

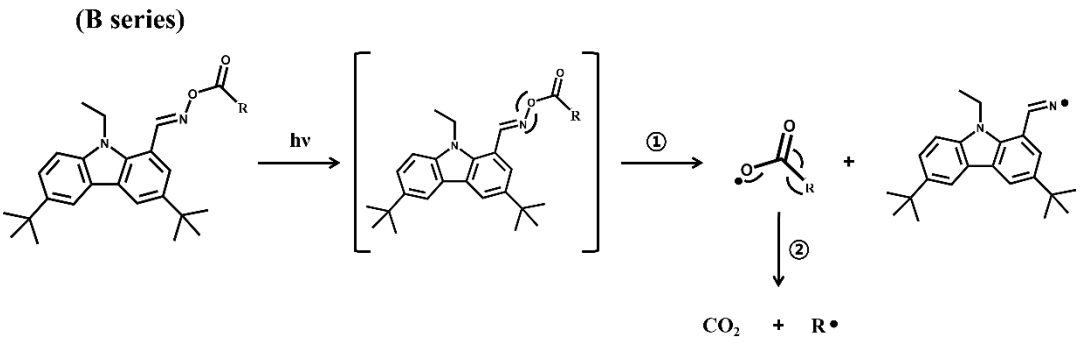

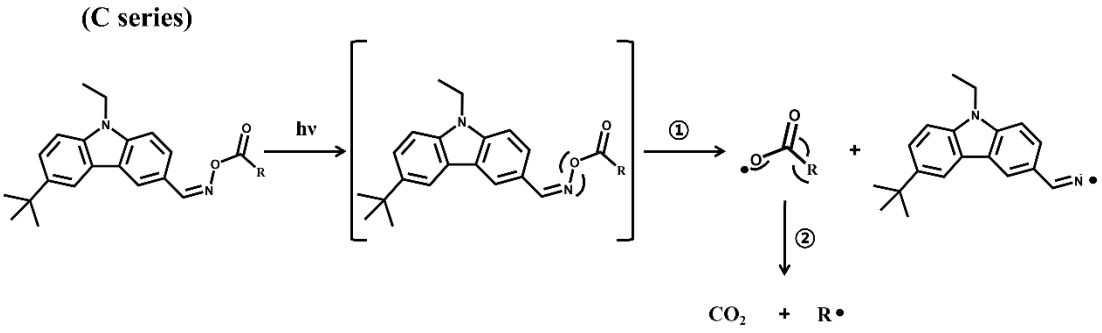

Scheme 2. Proposed Photoinitiation Mechanism of B series OXEs and C series OXEs.

3.8 3D printing experiments

OXEs showed good photoinitiation abilities in photopolymerization of TMPTA. Taking B8/TMPTA system as an example, applications of this photoinitiating system in 3D printing experiments were tested. As shown in Figure 9, the letter patterns "FNG" were successfully obtained in 2 minutes by DLW. The letter pattern showed a high spatial resolution (See Figure 10) and neat edges, which indicates that the printing effect was good.

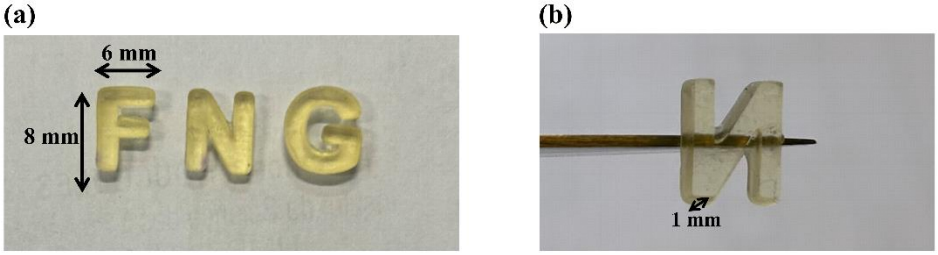

Figure 9. Digital photos of DLW objects using B8/TMPTA.

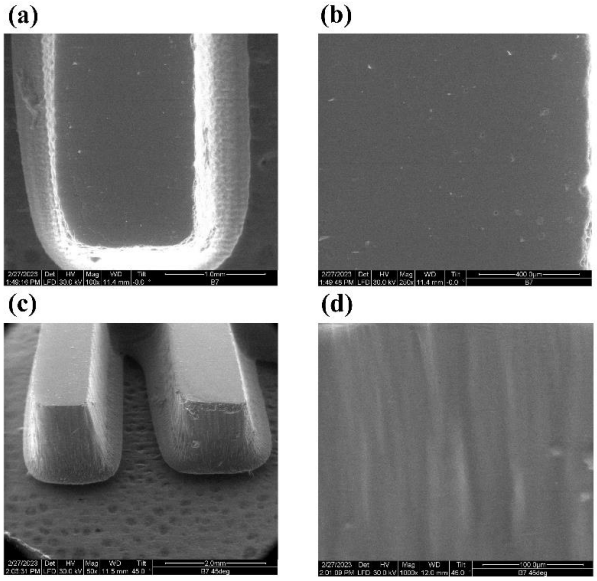

Figure 10. SEM images of surface of DLW objects using B8/TMPTA system.

4. Conclusion

Twenty-two novel OXEs bearing different functional groups (13 in the B series and 9 in the C series) were designed and synthesized for the first time. At room temperature, most OXEs showed good light absorption properties and photolysis under visible light irradiation. The photoinitiation ability was evaluated upon irradiation at 405 nm, and the results showed that some OXEs could initiate the polymerization of TMPTA efficiently. Interestingly, comparison of the photoinitiating abilities of the two series of oxime esters at 405 nm revealed the B series to outperform the C series. It can be concluded that the introduction of the photocleavable group in conjugated position with respect to the carbazole backbone favorably affects the reactivity of the oxime esters. Moreover, the interaction of the group with the chromophore leads to significantly shifted absorption properties depending on the position. Notably, OXE-B7 and OXE-B8 could be efficiently used to manufacture 3D objects with direct Laser write technology due to their high photoinitiating abilities. In addition, investigation of the photoinitiation mechanism of these OXEs showed that the N-O bond could cleave, generating acyloxy and iminyl radicals. By decarboxylation of acyloxy groups, CO_2 could be released and free radicals could be produced. In this study, the good photoinitiation abilities of OXEs were proved by theoretical calculations, RT-FTIR and

ESR-ST techniques. This work provides interesting tools for designing new high-performance oxime ester photoinitiators in the future.

Conflicts of interest

The authors declare no competing financial interest.

Acknowledgements

This research project is supported by China Scholarship Council (CSC) (No.202208220049).

References

[1] Y. Li, U. Shaukat, S. Schlögl, T. Xue, J. Li, J. Nie, X. Zhu, *European Polymer Journal* **2023**, *182*.

[2] W. Liao, Q. Liao, Y. Xiong, Z. Li, H. Tang, *Journal of Photochemistry and Photobiology A: Chemistry* **2023**, *435*.

[3] Z. Tang, Y. Gao, S. Jiang, J. Nie, F. Sun, *Progress in Organic Coatings* **2022**, *170*.

[4] X. Li, Z. Liu, P. Hong, L. Chen, X. Liu, *Progress in Organic Coatings* **2020**, *141*.

[5] X. Guo, W. Wang, D. Wan, M. Jin, *European Polymer Journal* **2021**, *156*.

[6] K. Dietliker, R. Hüsler, J. L. Birbaum, S. Ilg, S. Villeneuve, K. Studer, T. Jung, J. Benkhoff, H. Kura, A. Matsumoto, H. Oka, *Progress in Organic Coatings* **2007**, *58*, 146.

[7] A. E. Egorov, A. A. Kostyukov, D. A. Shcherbakov, D. A. Kolymagin, D. A. Chubich, R. P. Matital, M. V. Arsenyev, I. D. Burtsev, M. G. Mestergazi, E. R. Zhiganshina, S. A. Chesnokov, A. G. Vitukhnovsky, V. A. Kuzmin, *Polymers (Basel)* **2022**, *15*.

[8] K. Sun, X. Peng, Z. Gan, W. Chen, X. Li, T. Gong, P. Xiao, *Catalysts* **2022**, *12*.

[9] B. Ozkan, F. Sameni, S. Karmel, D. S. Engstrøm, E. Sabet, *Journal of the European Ceramic Society* **2023**, *43*, 1649.

[10] M. Regehly, Y. Garmshausen, M. Reuter, N. F. Konig, E. Israel, D. P. Kelly, C. Y. Chou, K. Koch, B. Asfari, S. Hecht, *Nature* **2020**, *588*, 620.

[11] W. Liao, M. Jin, *European Polymer Journal* **2023**, *187*.

[12] R. Acosta Ortiz, R. Yanez Macias, J. J. Ku Herrera, A. E. Garcia Valdez, *Polymers (Basel)* **2022**, *15*.

[13] M. Mohseni, S. Bastani, X. Allonas, S. Moradian, C. Ley, C. Croutxé-Barghorn, E. Mohajerani, *Progress in Organic Coatings* **2018**, *115*, 65.

[14] P. Xiao, J. Zhang, F. Dumur, M. A. Tehfe, F. Morlet-Savary, B. Graff, D. Gigmes, J. P. Fouassier, J. Lalevée, *Progress in Polymer Science* **2015**, *41*, 32.

[15] J. Radebner, A. Eibel, M. Leypold, C. Gorsche, L. Schuh, R. Fischer, A. Torvisco, D. Neshchadin, R. Geier, N. Moszner, R. Liska, G. Gescheidt, M. Haas, H. Stueger, *Angew Chem Int Ed Engl* **2017**, *56*, 3103.

[16] T.-L. Huang, Y.-C. Chen, *Journal of Photochemistry and Photobiology A:*

Chemistry **2022**, *429*.

[17] Y.-H. Li, Y.-C. Chen, *Polymer Chemistry* **2020**, *11*, 1504.

[18] W. Wang, M. Jin, H. Pan, D. Wan, *Progress in Organic Coatings* **2021**, *151*.

[19] S. Fan, X. Sun, X. He, Y. Pang, Y. Xin, Y. Ding, Y. Zou, *Polymers (Basel)* **2022**, *14*.

[20] C. Gao, J. Zeng, X. Zhang, Y. Liu, Z. P. Zhan, *Org Lett* **2023**, *25*, 3146.

[21] Y. Miyake, H. Takahashi, N. Akai, K. Shibuya, A. Kawai, *Chemistry Letters* **2014**, *43*, 1275.

[22] Z.-H. Lee, F. Hammoud, A. Hijazi, B. Graff, J. Lalevée, Y.-C. Chen, *Polymer Chemistry* **2021**, *12*, 1286.

[23] H. B. Mahmoud Rahal, Sylvain Duval, Bernadette Graff, Tayssir Hamieh, Joumana Toufaily, Frédéric Dumur, Jacques Lalevée, *European Polymer Journal* **2022**, *177*.

[24] Z. H. Lee, S. C. Yen, F. Hammoud, A. Hijazi, B. Graff, J. Lalevee, Y. C. Chen, *Polymers (Basel)* **2022**, *14*.

[25] S. Gong, X. Wu, Q. Liao, S. Deng, J. Hou, K. Tang, Y. Xiong, Z. Li, H. Tang, *Green Chemistry* **2023**, *25*, 2730.

[26] X. Ma, R. Gu, L. Yu, W. Han, J. Li, X. Li, T. Wang, *Polymer Chemistry* **2017**, *8*, 6134.

[27] Y. Ding, S. Jiang, Y. Gao, J. Nie, H. Du, F. Sun, *Macromolecules* **2020**, *53*, 5701.

[28] D. E. Fast, A. Lauer, J. P. Menzel, A.-M. Kelterer, G. Gescheidt, C. Barner-Kowollik, *Macromolecules* **2017**, *50*, 1815.

[29] L. Breloy, R. Losantos, D. Sampedro, M. Marazzi, J.-P. Malval, Y. Heo, J. Akimoto, Y. Ito, V. Brezová, D.-L. Versace, *Polymer Chemistry* **2020**, *11*, 4297.

[30] Z. Li, X. Zou, F. Shi, R. Liu, Y. Yagci, *Nat Commun* **2019**, *10*, 3560.

[31] Y. Wu, C. Dai, J. Ke, R. Tang, C. Huang, J. Wang, Y. Situ, H. Huang, *Progress in Organic Coatings* **2023**, *176*.

[32] Y. G. Yijun Zhang, Ludovic Josien, Habiba Nouali, Cyril Vaulot, Angélique Simon-Masseron, Jacques Lalevée, *Advanced Materials Technologies* **2021**.

[33] W. Wang, M. Jin, H. Pan, D. Wan, *Dyes and Pigments* **2021**, *192*.

[34] W. Qiu, M. Li, Y. Yang, Z. Li, K. Dietliker, *Polymer Chemistry* **2020**, *11*, 1356.

[35] S. Kato, H. Noguchi, A. Kobayashi, T. Yoshihara, S. Tobita, Y. Nakamura, *J Org Chem* **2012**, *77*, 9120.

[36] Y. Zhang, F. Morlet-Savary, M. Schmitt, B. Graff, A. Rico, M. Ibrahim-Ouali, F. Dumur, J. Lalevée, *Dyes and Pigments* **2023**, *215*.

[37] F. Hammoud, G. Noirbent, B. Graff, A. Hijazi, M. Nechab, D. Gigmes, F. Dumur, J. Lalevée, *Mater. Chem. Front* **2021**, *5(24).* 8361.

488 **TOC graphic:**

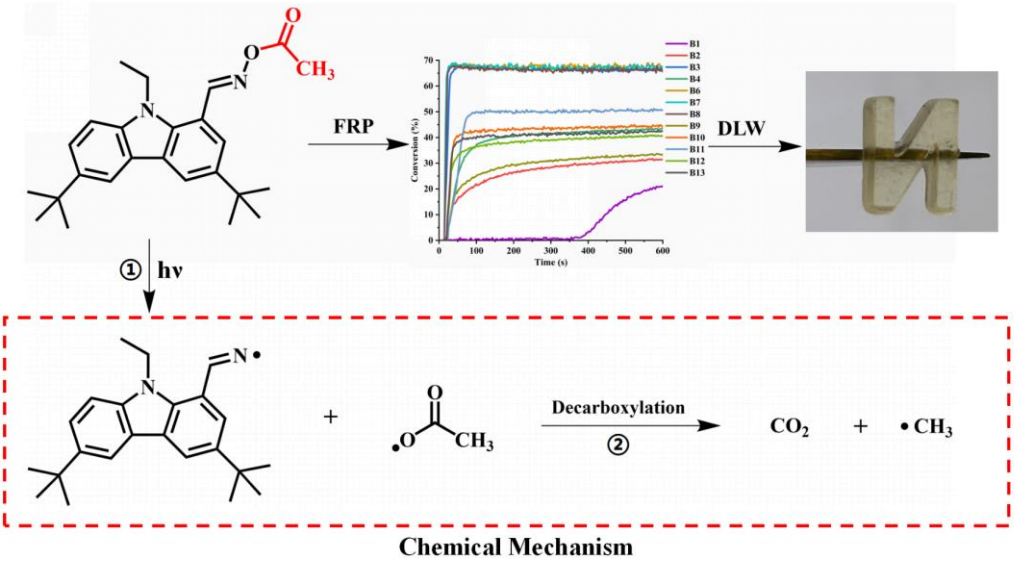

Chemical Mechanism

489

490

491